IEEE Access
Multidisciplinary ⋮ Rapid Review ⋮ Open Access Journal

Received 30 November 2023, accepted 25 December 2023, date of publication 3 January 2024,
date of current version 11 January 2024.

Digital Object Identifier 10.1109/ACCESS.2024.3349402

RESEARCH ARTICLE

Grid-Connected PV Inverter for Driving Induction Machines With Synchronous Scalar Control

KANGBEEN LEE[1], (Graduate Student Member, IEEE),
MOSTAFA FEREYDOONIAN[1], (Graduate Student Member, IEEE),
MIKAYLA BENSON[1], (Graduate Student Member, IEEE),
AVINASH DORNALA[1], (Graduate Student Member, IEEE),
MUSAB GUVEN[1], (Graduate Student Member, IEEE),
YOUNSUK DONG[2], (Member, IEEE), AND
WOONGKUL LEE[1], (Member, IEEE)
[1]Department of Electrical and Computer Engineering, Michigan State University, East Lansing, MI 48864, USA
[2]Department of Biosystems and Agricultural Engineering, Michigan State University, East Lansing, MI 48864, USA

Corresponding author: Kangbeen Lee (leekangb@msu.edu)

This work was supported under the MTRAC Program by the State of Michigan 21st Century Jobs Fund received through the Michigan Strategic Fund and administered by the Michigan Economic Development Corporation.

ABSTRACT Induction machines (IMs) are used extensively in irrigation systems due to their high reliability and line-starting capability directly from the power grid without requiring variable speed drives (VFDs). Nonetheless, line-connected IMs draw a substantial starting current from the grid, leading to grid instability, heightened demand charges, and premature failures in irrigation systems due to excessive water pressure. Although VFDs can effectively alleviate the starting current, their associated costs for equipment, installation, and maintenance are higher than line-connected IMs. Consequently, this results in limited adoption in the market. This paper proposes a shunt-connected photovoltaic (PV) inverter with a newly devised synchronous scalar control technique to tackle this issue. This system can be retrofitted into existing line-connected IM setups to reduce the excessive initial current effectively. Once the IM attains its rated operating state, the power source is seamlessly switched from the PV inverter to the power grid within two electrical cycles. This minimizes transient currents while ensuring uninterrupted operation of the irrigation system. The PV inverter can supply continuous active and reactive power, resulting in energy savings throughout the year during irrigation and off-irrigation seasons. Moreover, the proposed PV inverter can be dimensioned as small as 50% of the irrigation system, significantly reducing the peak starting current. Simulation and experimental results closely align, demonstrating the favorable soft-starting performance of the inverter.

INDEX TERMS Induction machine, irrigation, PV inverter, scalar control, soft-starting, starting current.

I. INTRODUCTION

Most agricultural irrigation systems are centered around a pump, and it is essential to ensure that the pump is appropriately sized to match the requirements of the water source, distribution network, and demands of irrigation equipment. However, it is estimated that around 75% of existing irrigation pump systems are generally oversized by more than 20%. This oversizing ensures these systems can lead to high flow rates and pressures at the pump [1], [2], [3].

The variable speed drives (VFDs) offer an effective solution for matching pump systems more precisely to the actual requirements of the irrigation setup. This leads to energy savings and conserves a significant amount of water. Nevertheless, there are currently approximately 20 times more fixed-speed (line-connected) induction machine (IM)-driven pumps in operation compared to the number of new ones entering the market each year. This slow adoption rate can be attributed to the challenges associated with replacing existing

The associate editor coordinating the review of this manuscript and approving it for publication was Ton Duc Do.

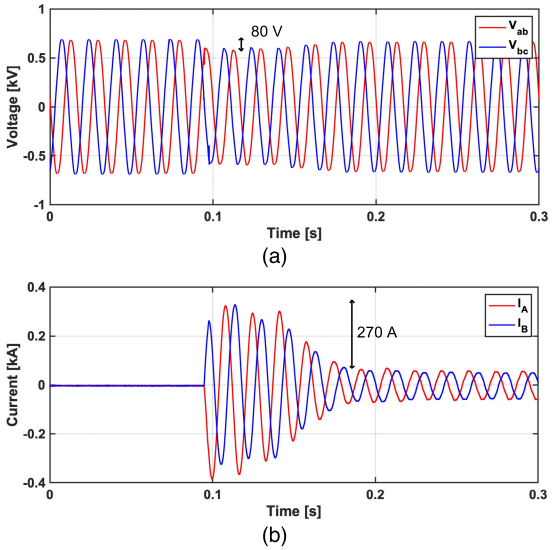

FIGURE 1. Measured power grid (a) line-to-line voltage drop of 80 V (480 V_{rms}) and (b) over 330 A peak starting current of a line-connected IM (50 hp).

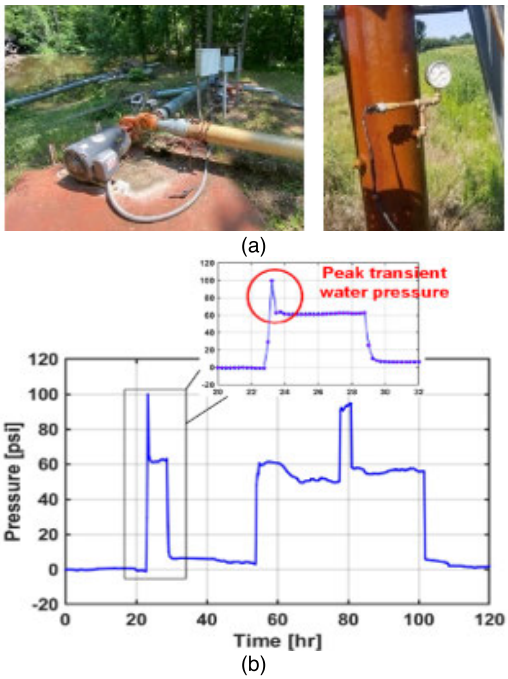

FIGURE 2. Measured water pressure from a line-connected induction machine-driven irrigation pump for five days (124 hours) with 15 minutes sampling interval. (a) Measured pressure data. (b) Demonstration site with IM-driven irrigation pump and pressure sensor.

systems with VFDs, which involve substantial costs and time investments [4].

Due to the numerous merits associated with IMs, such as their mechanical simplicity, durability, reliability, cost-effectiveness, and low maintenance requirements, they have traditionally dominated the landscape of irrigation systems. However, the line-connected IM presents a significant challenge during its starting phase, requiring an excess of 7 per unit (p.u.) starting current, as depicted in Figure 1(a) and (b). This excessive starting current can result in power grid instability, elevated demand charges, and a decline in the reliability of the irrigation system [5].

It is crucial to note that this high starting current also generates substantial starting torque, causing the water pressure in the irrigation system to soar to levels as high as 100 pounds per square inch (psi). This is 40 psi higher than the nominal operating condition, as displayed in Figure 2(a). This undesirable surge in water pressure, often called water hammer, can lead to premature failure of the irrigation system and necessitate more frequent maintenance [6], [7], [8], [9], [10].

To mitigate the high starting current problem of IMs, the V/Hz control (i.e., scalar control) is widely used as a simple and robust induction machine control approach. It is proved that the V/Hz control with the compensated slip frequency from a nonlinear torque-speed approximation reduces the speed error, leading to starting a current reduction [11]. A new control algorithm for V/Hz control of pulse width amplitude modulation (PWAM) with a multilevel quasi Z source inverter (qZSI) achieves starting of IM without the starting current transient [12]. The V/Hz control also opened a door for cost-effective restarting of IM when IM operation should be re-initiated due to momentary power disruptions. A V/Hz fuzzy-logic control mechanism that ensures the alignment of the output frequency with machine speed is proposed in [13]. This is achieved even when knowledge of machine parameters or speed feedback is unavailable when the machine is in a field-weakening state. Furthermore, a universal flying restart strategy of the IM using V/Hz control was proposed in [14], [15], and [16]. The strategy using input power and input power perturbation effectively resolves the instability and searching time concerns associated with the integrator controller in identifying rotor speed. The restarting methods with the V/Hz control under a single power source have been proposed and proved their validity, but a V/Hz control synchronized with two different power sources, such as photovoltaic (PV) inverter and AC power grid, has not been investigated.

This paper introduces a shunt-connected PV inverter system with a newly proposed synchronous V/Hz control method, which provides voltage and angle synchronization during the transition between PV inverter and AC power grid. The proposed system can be readily retrofitted into existing line-connected IMs, and effectively mitigates the high starting current, as outlined in [1], [17], and [18]. Moreover, when the irrigation season concludes, this PV inverter can be reconfigured to a standard PV inverter, providing continuous active and reactive power throughout the year and resulting in substantial energy savings.

Section II will introduce the proposed shunt-connected PV inverter topology and its operating principle. Section III introduces the commutation strategies of four different modes of operation, relay configuration, and dead time. Section IV will present the proposed synchronous scalar control technique, which synchronizes the V/Hz control with the power grid.

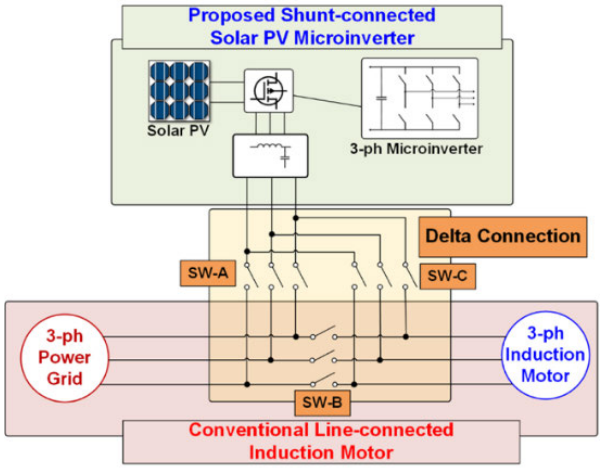

FIGURE 3. Proposed shunt-connected PV inverter and 3-phase power system grid connection for IM-driven irrigation pump.

Section V will provide the estimated starting current simulation results with different active and reactive power levels injected from the shunt-connected PV inverter. Section VI will show the experimental results. The conclusion will be drawn in the last section.

II. PROPOSED SHUNT-CONNECTED PV INVERTER TOPOLOGY AND OPERATING PRINCIPLE

The suggested shunt-connected PV inverter system comprises several key components: a PV panel, a three-phase inverter, a line filter (such as an LC or LCL filter), and a delta-connected relay system for reconfiguration, as visually represented in Figure 3. This PV inverter is linked in parallel (shunt-connected) with the current line-connected IM system, which encompasses the power grid, a three-phase IM, and relay systems using the delta-connected relay setup.

In typical grid-tied applications, a three-port wye-connected relay configuration utilizing mechanical AC contactors [19], [20], [21], [22] is commonly employed, featuring a single point of common coupling (PCC), as demonstrated in Figure 4(a). Nevertheless, this wye-connected relay arrangement is associated with elevated conduction losses due to the series connection of two contactors in each mode of operation.

In contrast, the proposed three-port delta-connected relay configuration necessitates only one contactor for each mode, thereby reducing the overall conduction loss by 50%, as delineated in Figure 4(b). It's crucial to emphasize that integrating the PV inverter into the system as a shunt connection requires minimal modifications, making it easily retrofittable into the existing line-connected IM-based irrigation system. This approach results in savings on initial installation and replacement costs.

An irrigation pump and IM typically have power ratings ranging from a few horsepower to several tens of horsepower (e.g., 5 – 60 hp). The specific rating depends on factors such as the size of the farm and the type of crops being cultivated [23], [24], [25]. Consequently, a single unit of the PV inverter module is optimally designed with a 6.5 hp (5 kVA) capacity, and the overall power rating can be expanded by connecting multiple modules in parallel. For instance, it can cover a wide range of irrigation systems. A comprehensive specification for a solitary PV inverter module is provided in Table 1, with the inverter designed for operation with a 240 V_{rms} three-phase power grid.

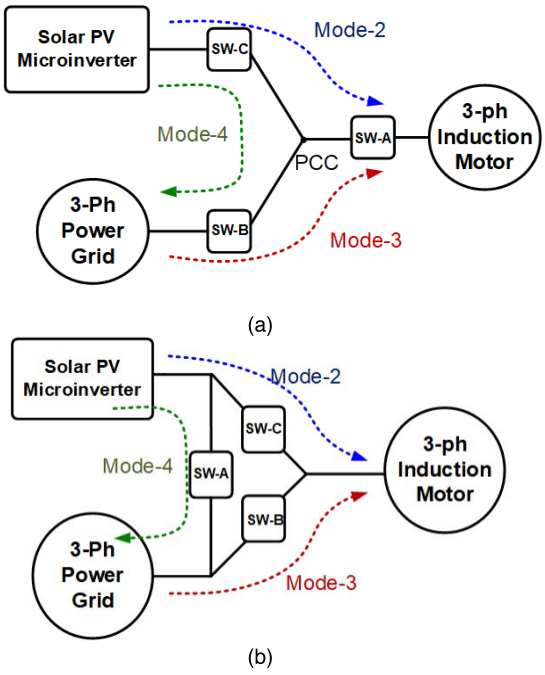

FIGURE 4. Two three-port relay configurations for the proposed shunt-connected PV inverter (a) Wye-connected, (b) Delta-connected relays (proposed).

TABLE 1. Specification of the PV inverter and PV panels for MATLAB simulink simulation.

Parameters	Value	Unit
Inverter output power	5	kVA
DC-link voltage	440	V
Single PV panel maximum power	370	W
Single PV panel MPP voltage	37	V
Number of PV panels for a string	12	-
PV string power	4.4	kW
PV string MPP voltage	440	V
PV string MPP current	10.01	A
Grid voltage	240	V_{rms}

The shunt-connected PV inverter can operate in four distinct modes, and the delta-connected relay system, which can be comprised of either mechanical or solid-state contactors, facilitates seamless transitions among these modes. A complete operational cycle necessitates sequential transitions from Mode 1 to Mode 4, as succinctly detailed in Table 2.

Mode 1 signifies an idle state with no power flow, where neither the PV inverter nor the power grid is connected to the IM. In Mode 2, the PV inverter links to the IM

TABLE 2. Four different modes of operation of the proposed shunt-connected PV inverter.

Mode of Operation	Power Flow	Functions
Mode 1	No power flow	Idle
Mode 2	PV inverter → Induction machine	Induction machine soft-starting
Mode 3	Power grid / PV inverter → Induction machine	Peak shaving and reactive power compensation
Mode 4	PV inverter → Power grid	Renewable energy generation

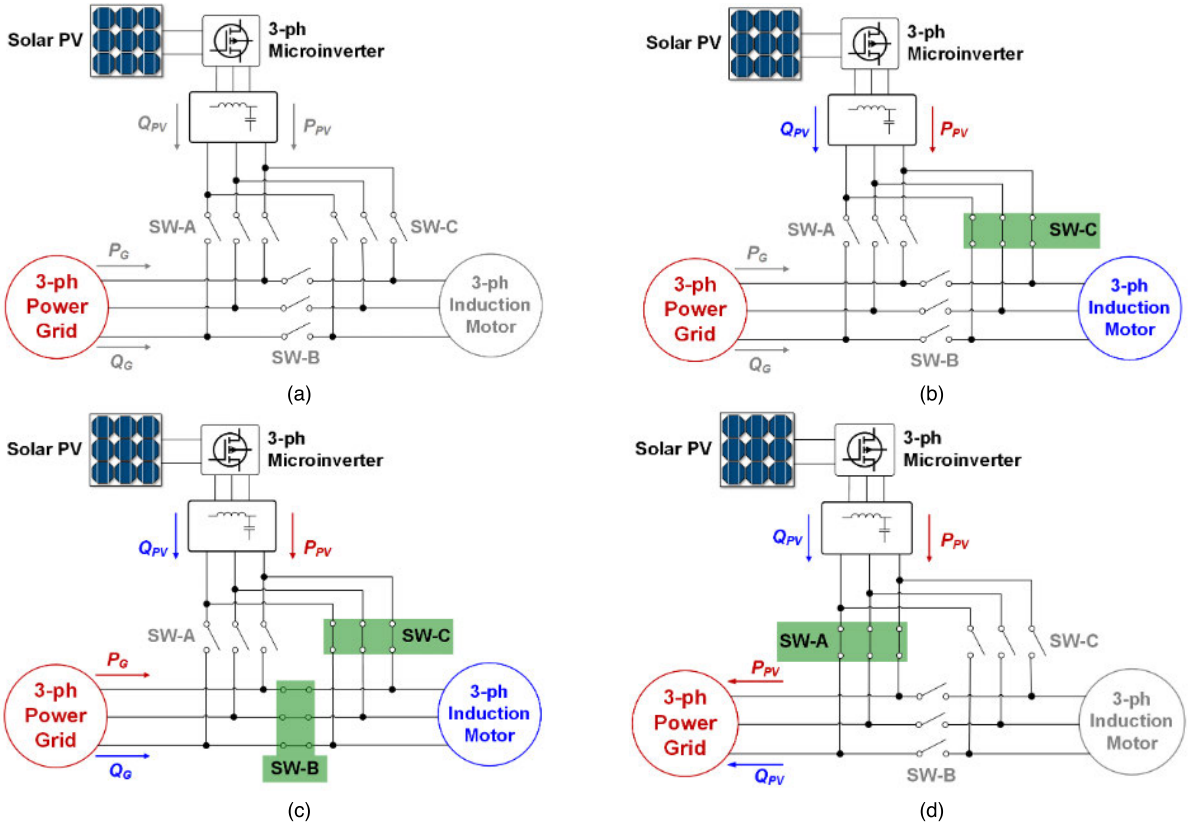

FIGURE 5. Four modes of operation of the shunt-connected PV inverter system. (a) Mode 1 - idling, (b) Mode 2 - IM soft-starting, (c) Mode 3 - peak shaving and reactive power compensation, (d) Mode 4 - regular PV inverter operation mode (off-irrigation season).

for a soft start using a synchronous scalar control technique. Importantly, this technique does not require the installation of additional rotor position sensors, such as encoders, hall sensors, or resolvers. When the IM reaches its rated speed, the power source switches back to the power grid for continuous IM operation in Mode 3. During this mode, the PV inverter may continue to supply active or reactive power to the power grid for peak shaving and reactive power compensation.

Although the PV inverter can provide sufficient power for IM operation, Mode 3 is vital for ensuring the uninterrupted operation of the irrigation system, taking into account the intermittent and variable nature of solar energy. In Mode 4, the proposed PV inverter system directly connects to the power grid to generate active and reactive power, promoting year-long energy savings through typical renewable energy generation practices.

III. COMMUTATION AND RECONFIGURATION PROCESS

As the proposed shunt-connected PV inverter necessitates transitions between its four operational modes, executing the commutation process with proper consideration for the dead time between these modes is crucial. In Mode 1, both the shunt-connected PV inverter and the power grid are disconnected from the IM, resulting in zero power flow, as shown in Figure 5(a). Contactor C (SW-C) is closed to activate the irrigation pump, enabling the shunt-connected PV inverter to drive the IM using the synchronous scalar control technique. This eliminates the high peak starting current, as depicted in Figure 5(b), marking the transition to Mode 2.

Moving from Mode 2 to Mode 3 occurs when the IM achieves a stable operational state. Initially, the PV inverter is temporarily disengaged, providing no power to the IM. While the IM continues to rotate with its inherent inertia, the grid-side contactor (SW-B) is closed, facilitating the transition from Mode 2 to Mode 3 within a brief period of two electrical cycles (less than 35 ms). This swift transition ensures uninterrupted operation of the irrigation pump, unaffected by weather conditions or temporary shading issues with the PV panels. Following the completion of

this transition, the PV inverter can supply active and reactive power to the IM to support the power grid, as illustrated in Figure 5(c).

Upon concluding the irrigation pump operation, only contactor A (SW-A) is engaged, directly connecting the PV inverter to the power grid, as displayed in Figure 5(d), denoting the initiation of Mode 4. In this mode, the PV inverter is capable of delivering active and reactive power, facilitating year-round energy savings, particularly during the fall and winter seasons when the irrigation season is inactive.

IV. SYNCHRONOUS SCALAR CONTROL TECHNIQUE

One of the key benefits of the proposed shunt-connected PV inverter is that this system can be retrofitted to the line-connected IM-drive irrigation pumps without any significant modification to the existing irrigation system. Since most line-connected IMs do not have rotor position estimation sensors such as an encoder or resolver, the PV inverter utilizes a scalar control technique (i.e., V/Hz control) to keep the starting current constant during the machine acceleration. However, the conventional scalar control, shown in Figure 6(a), does not provide the grid synchronization capability, which is critical when the mode of operation changes from Mode 2 to 3. The conventional scalar control calculates the three-phase output voltages from the input frequency and the corresponding voltage commands,

$$v_a = V_s^* sin(2\pi f_s^* t) \tag{1}$$
$$v_b = V_s^* sin(2\pi f_s^* t + 2\pi/3) \tag{2}$$
$$v_c = V_s^* sin(2\pi f_s^* t - 2\pi/3) \tag{3}$$

where f_s* is the input command frequency, and V_s* is the calculated PV inverter output voltage command.

When the IM operates in its rated condition, the PV inverter output voltage is at its peak and an identical frequency with the power grid. To ensure minimum transient current from the power grid, the angle difference between the PV inverter output voltage and the power grid voltage must ideally be zero.

For the grid and PV inverter output voltage synchronization, a new synchronous scalar control technique is proposed in this paper as shown in Figure 6(b). Instead of using the conventional scalar control technique where the input frequency (f_s^*) is used to estimate the input voltage magnitude (V_s^*) through a predefined V/Hz waveform, the frequencies of three-phase output voltages are calculated using the grid voltage and expressed as,

$$\theta_{grid} = 2\pi f_{grid} t \tag{4}$$
$$v_a = V_s^* sin(k\theta_{grid}) \tag{5}$$
$$v_b = V_s^* sin(k\theta_{grid} + 2\pi/3) \tag{6}$$
$$v_c = V_s^* sin(k\theta_{grid} - 2\pi/3) \tag{7}$$
$$k = \frac{f_s^*}{f_{grid}} \tag{8}$$

where θ_{grid} is the power grid angle estimated through phase locked loop (PLL), f_{grid} is the grid frequency, and V_s* is the calculated PV inverter output voltage command. Since the estimated grid angle is directly used to calculate the PV inverter output voltage, the final output of the synchronous scalar control technique is synchronized with the grid output voltage in its frequency and angle, when k is equal to 1 as shown in Figure 6(c). The grid synchronization capability of the proposed synchronous scalar control technique is validated through simulation and experiment in the following sections.

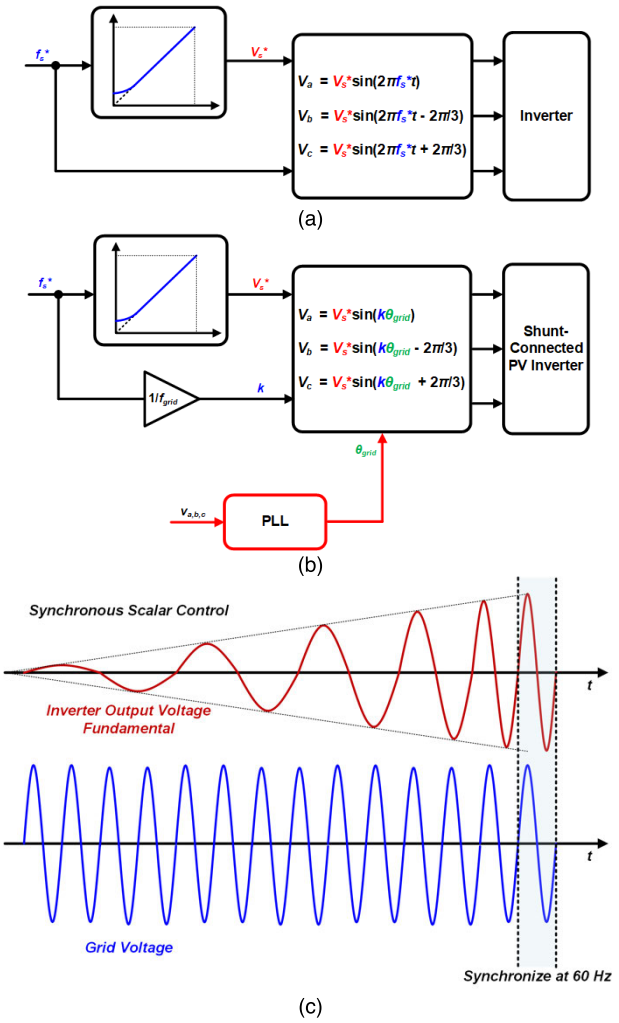

FIGURE 6. Controller diagram of (a) the conventional scalar control and (b) the proposed synchronous scalar control technique with grid synchronization. (c) Inverter output voltage synchronizing with grid voltage at 60 Hz through synchronous scalar control technique.

V. SIMULATION RESULTS

A. OPTIMAL DEAD TIME SELECTION

To guarantee a smooth transition between various operational modes and to alleviate potential concerns such as transient currents and short circuits, it is essential to precisely adjust the dead time in the relay setup of the PV inverter system. The dead time represents the duration between the deactivation of one relay and the activation of the next.

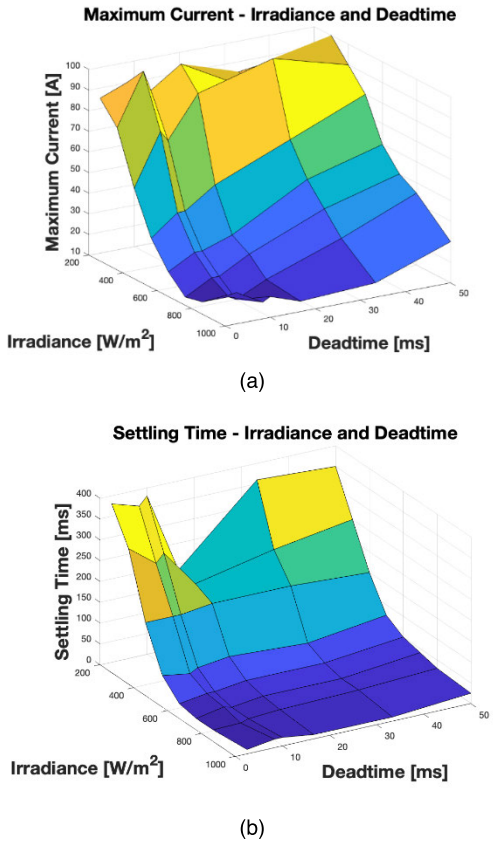

FIGURE 7. Maximum current and settling time of the three-phase power grid with respect to different dead times and irradiances.

A parametric analysis was conducted to assess this comprehensively, encompassing a wide range of irradiances spanning from 200 to 1,000 W/m^2, alongside different dead time values ranging from 0 to 50 ms. The primary objective of this analysis was to quantify the maximum current and the setting time of the input current for the IM. The outcomes of this analysis are presented in Figure 7. As anticipated, the maximum transient current diminishes as the dead time is reduced and the irradiance levels increase. For instance, below 20 A is observed within the small dead time range of 0 to 20 ms and under high irradiance conditions ranging from 800 to 1,000 W/m^2, as depicted in Figure 7(a). Given that the maximum current experiences an uptick within the dead time range of 0 to 10 ms, the optimal dead time interval is determined to be between 10 to 20 ms.

Solar irradiance plays a pivotal role in determining the system's settling time, while it exhibits a limited sensitivity to variations in the dead time, as illustrated in Figure 7(b). In order to minimize the settling time, it is suggested that an optimal dead time range of 10 to 30 ms be considered. However, when taking into account both the maximum current and the settling time, the optimal dead time narrows down to the 10 - 20 ms range.

This selected optimal dead time configuration ensures that the system experiences a minimal peak transient current falling within the 10 to 20 A range and achieves

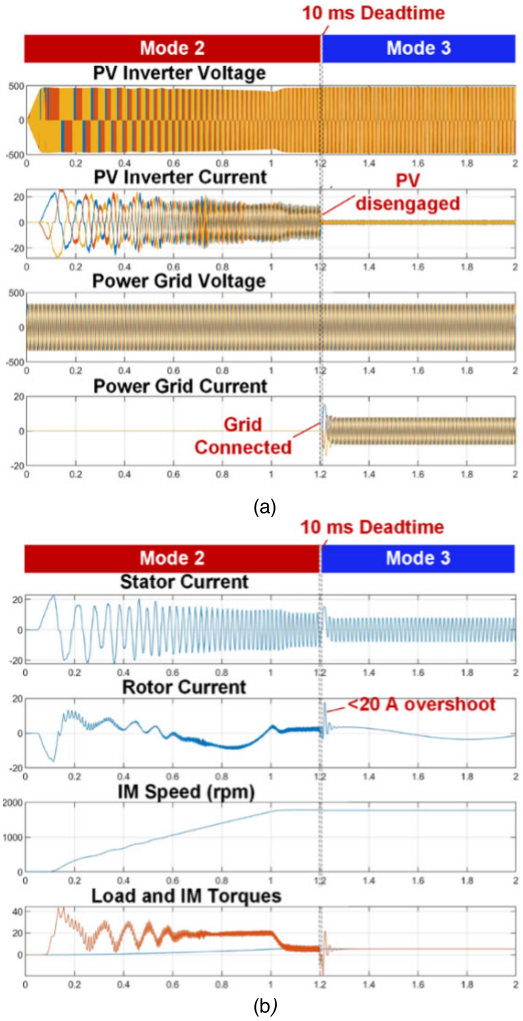

FIGURE 8. Simulated PV inverter for induction machine soft-starting with 10 ms dead time and transition from Mode 2 to 3. (a) Estimated output voltage and current of the PV inverter and power grid at 100% irradiance. (b) IM current, speed, and torque characteristics during the starting and mode transition.

settling within less than 30 ms when the solar irradiance surpasses 500 W/m^2. It's noteworthy that this proposed dead time range aligns with the typical switching time of mechanical relays, which typically falls between 10 to 20 ms. This finding validates that operators of irrigation systems can effectively employ the proposed shunt-connected PV inverter to reduce the starting current during a substantial time window exceeding 12 hours, for instance, from 6 a.m. to 6 p.m.

B. STARTING CURRENT EVALUATION AND DEAD TIME EFFECT

The proposed shunt-connected PV inverter, the delta-connected relay configuration, and the three-phase power grid system were modeled and simulated via MATLAB Simulink. In the initial analysis, the PV inverter supplied 1 p.u. output power to the IM during Mode 2, resulting in a soft start with a starting current of less than 25 A, as depicted in Figure 8(a). The synchronous scalar control technique

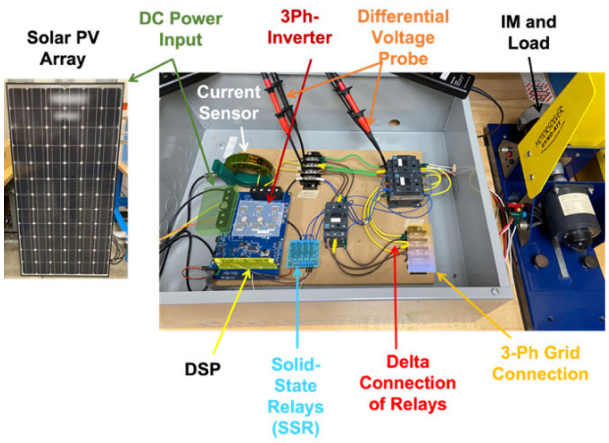

FIGURE 9. Experimental setup of the proposed shunt-connected PV inverter and IM.

ensured that the stator current and machine torque remained relatively constant while the machine speed linearly increased until reaching its rated value of 1,750 rpm, as illustrated in Figure 8(b).

The transition from Mode 2 to Mode 3 was facilitated with a 10 ms dead time, and the maximum transient current drawn from the power grid was below 20 A, as shown in Figure 8(a). Notably, the peak overshoot in the transition current was observed to be five times lower than the typical starting current of a line-connected IM, which exceeds 90 A.

VI. EXPERIMENTAL RESULTS

The experimental setup of the proposed shunt-connected PV inverter is designed and tested as shown in Figure 9. The synchronous scalar control method is implemented in the MATLAB Simulink, and autocode generation is used to load the code on the target digital signal processor (DSP). A three-phase machine drive (TMS320F28335 control-CARD and TI-DRV8301-HC-C2) is used for the PV inverter. The IM and the dynamometer are rated at 200 W for lab-scale testing and demonstration. A three-phase grid simulator model 9410 from NHR is used for the power grid. The IM and three-phase inverter specifications are summarized in Table 3. The selected mechanical relays were rated at a phase voltage of 240 V_{rms} to be retrofitted to the existing line-connected system. The mechanical relay input signals are provided by a four-channel optically isolated solid-state relay (SSR), which serves as an interface between the DSP and the delta-connected relays.

A. DEAD TIME ESTIMATION OF MECHANICAL RELAYS

To achieve the most efficient operation of the proposed PV inverter with minimal transient and settling times, the relay switching speed was assessed to determine the times it takes for the relays to turn on and off. The cumulative dead time of the delta-connected relay within the PV inverter system relies on the turn-off time of SW-C and the turn-on time of SW-B, which is less than 20 ms, as evident in Figure 10(a) and (b).

TABLE 3. Experimental setup specifications.

Parameters	Value	Units
Rated power	200	W
Rated voltage	20	V_{rms}
Max speed	4,000	RPM
Number of poles	4	-
Rotor moment of inertia	5.89×10^{-5}	$Kg\cdot m^2$
Resistance (L-L)	0.32	Ω
Grid voltage	20	V_{rms}
Grid frequency	60	Hz
Inverter DC-link Voltage	25	V
Inverter Power Rating	500	W

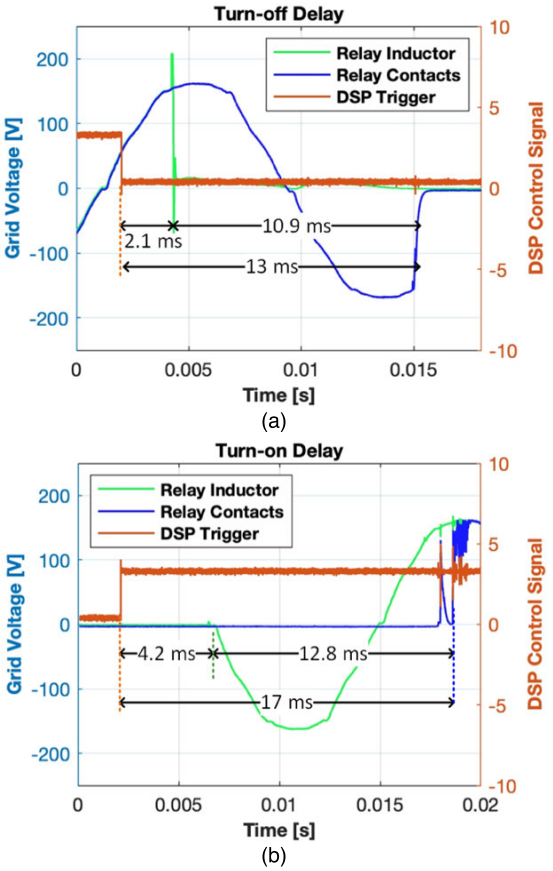

FIGURE 10. Measured timing of DSP signal, relay inductor turn-on and -off, and relay contactor turn-on and -off.

The total turn-off delay of the selected mechanical relay was measured at 13 ms, encompassing the delay between the DSP signal and the relay inductor and the interval between the relay inductor and the actual relay contactor turning off. Similarly, the total turn-on delay of the chosen mechanical relay was measured at 17 ms, encompassing the delay between the DSP signal and the relay inductor and the interval between the relay inductor and the actual relay contactor turning on.

This demonstrates that the combined dead time during the transition between modes can potentially be reduced to as low as 17 ms if the turn-on and turn-off commands are issued sequentially. While this dead time still falls within the

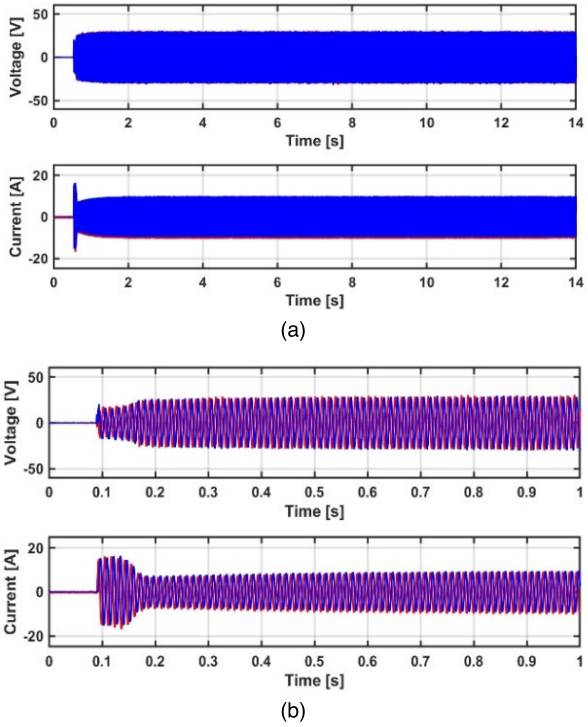

FIGURE 11. Measured grid voltage and IM stator current during line starting process. (a) Measured grid voltage and current for 14 s. (b) Zoom-in waveforms of grid voltage and current for 1 s.

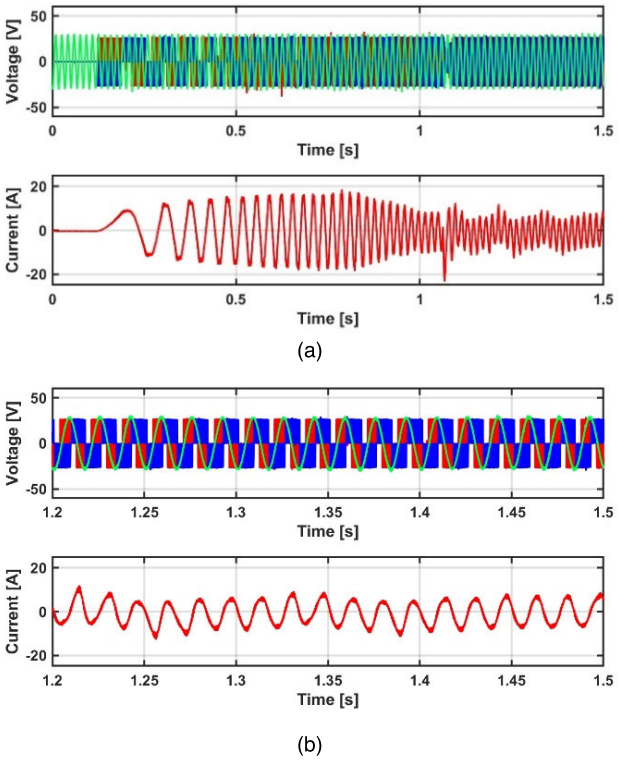

FIGURE 12. Measured PV inverter output voltage, current, and power grid voltage for grid synchronization. (a) PV inverter output voltage, current, and grid voltage for 1.5 s. (b) Zoom-in waveform of the PV inverter output voltage, current, and grid voltage in rated condition (steady-state).

optimal range of 10 to 20 ms, further reduction is possible by overlapping the turn-off and turn-on commands without causing a short circuit in both relays.

Given that the experimental setup represents a scaled-down model of irrigation pumps, typically rated at over 20 hp, there are variations in machine starting and rated current when compared to larger induction machines (IMs) operating at a fixed grid frequency. To compare the starting current with and without the proposed shunt-connected PV inverter, the IM starting current without the PV inverter is measured. This measurement uses a 200 W IM and a 20 V_{rms} grid voltage operating at 60 Hz.

In the case of an IM with a stationary rotor, it behaves akin to a transformer with a short-circuited secondary winding. In this scenario, there is no back electromotive force (emf) to counteract the emf in the stator windings. Consequently, a considerably high current flows through both the stator and rotor windings. As the rotor's speed increases, approaching the rated revolutions per minute (rpm), the back emf generated by the rotor leads to a reduction in stator current.

Figure 11(a) illustrates the grid voltage and stator/grid current during the process of line starting. A closer examination in Figure 11(b) reveals that the stator current surges to 16.5 A during the first five electrical cycles. After just 0.1 seconds, the IM stabilizes at a steady-state condition. It's worth noting that the grid voltage experiences a 30% drop as the IM draws a high starting current. This phenomenon aligns with the observations made in field measurements, as depicted in Figure 1(a) and (b).

B. SYNCHRONOUS SCALAR CONTROL FOR SOFT-STARTING AND GRID SYNCHRONIZATION

The proposed synchronous scalar control technique is executed within MATLAB Simulink, and autocode generation is employed to transform the model into the DSP code required for the target system. This generated code gently initiates the IM to validate two specific objectives: (1) achieving a soft start and (2) ensuring grid synchronization under rated conditions.

Using the PV inverter with the synchronous scalar control technique, variable frequencies, and pulse width output voltages are generated, as portrayed in Figure 12(a). Throughout the machine's acceleration phase, the PV inverter maintains the IM stator current at a peak value of less than 20 A through scalar control. This guarantees the soft start of the IM with the PV inverter and synchronous scalar control, minimizing the peak current.

Once the IM reaches its rated speed, verifying whether the PV inverter's output voltage is synchronized with the grid voltage to minimize grid transient currents is imperative. Figure 12(b) displays both phase A of the PV inverter's output voltage (in red) and the grid voltage (in green), confirming the synchronization of both waveforms.

TABLE 4. Experimental result comparison between conventional (line starting) and proposed topology with scalar control.

	Conventional	Grid-connected PV Inverter
Current Overshoot Rate [%]	98.56	80.51
Transition Time [Number of Cycles]	5	2

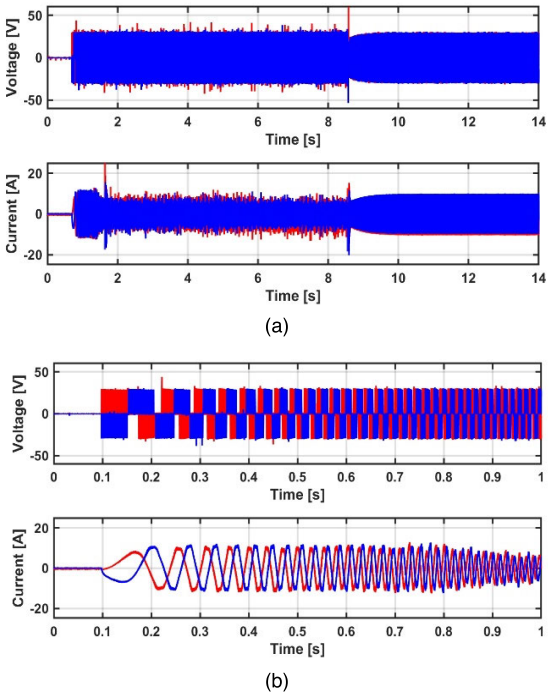

FIGURE 13. Full test results of the experimental setup. (a) Stator voltage and current for soft-starting and transition modes, (b) Zoom-in voltage and current waveforms during soft-starting.

C. DEMONSTRATION OF SOFT-STARTING AND MODE TRANSITION

The final demonstration encompasses two key aspects: the soft-starting of the IM and the operation transition from Mode 2 to Mode 3, as visually represented in Figures 13 and 14. In Figure 13(a), we observe the stator voltage and current of the IM over the entire test duration, which spans approximately 9 seconds. The proposed synchronous scalar control technique facilitates the gentle initiation of the IM using solar energy. Figure 13(b) illustrates that this soft-starting technique effectively regulates the IM's stator current to remain below 15 A during the acceleration phase.

Upon reaching its rated speed of 1,750 rpm, one of the three mechanical relays that connect the PV inverter with the IM is deactivated at around 7.955 seconds, as demonstrated in Figure 14(a). Following a 30 ms dead time, the power grid becomes engaged through the activation of the

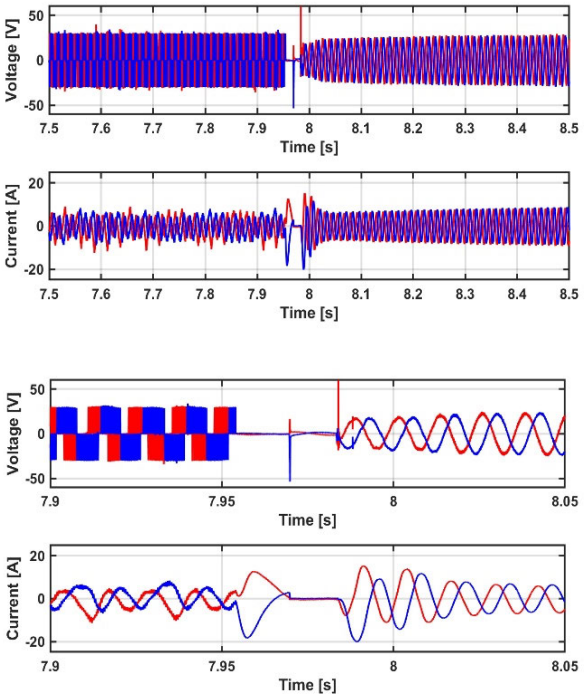

FIGURE 14. Full test results of experimental setup. (a) Mode transition from 2 to 3 with 30 ms deadtime, and (b) Zoom-in waveforms of transient voltage and current between Mode 2 and 3.

grid-side mechanical relay, ensuring the continuous operation of the IM. The recorded grid current exhibits a peak value of less than 15 A and settles within less than two electrical cycles. This starkly contrasts the line-starting IM operation, where the peak current exceeds 15 A, and the settling time extends beyond five electrical cycles, as shown in Figure 14 (b). In comparison, with its soft-starting technique, the proposed PV inverter effectively mitigates both the IM's starting current and settling time. The key experimental results of the comparison between the conventional system with line-starting and grid-connected PV inverter with the scalar control method (e.g., peak starting current of IM and number of cycles in the transition) are summarized in Table 4.

VII. CONCLUSION

This paper presents a novel shunt-connected PV inverter system that incorporates the PV inverter, synchronous scalar control, and delta-connected relay. The main objective of this system is to mitigate the high starting current of the IM by utilizing the PV inverter during the starting period. Four distinct modes of operation and commutation strategies are introduced, and the optimal dead time with minimum transient current is quantified through simulation. A comprehensive parametric analysis is conducted to identify the optimal dead time, irradiance, and inverter voltage that results in minimal transient current and settling time, which should

be less than 30 ms. An experimental setup is designed to validate the proposed system, and the turn-on and turn-off times of the mechanical relay are measured. The measured delay times are found to be 13 ms and 17 ms, respectively, falling within the optimal dead time range of less than 30 ms. By employing the optimal dead time and maintaining an irradiance level higher than 500 W/m^2, the proposed shunt-connected PV inverter system can reduce the peak transient current to as low as 20% of that observed in a conventional line-connected IM system. Additionally, the settling time can be reduced by 60%. Finally, a demonstration confirms the effectiveness of the proposed synchronous scalar control in facilitating a soft start of the IM and ensuring synchronization with the power grid during the rated operating condition, thereby minimizing transient current during mode transitions.

REFERENCES

[1] M. Guven, K. Lee, Y. Dong, and W. Lee, "Shunt-connected solar microinverter for induction motor soft-starting and active and reactive power compensation," in *Proc. IEEE Energy Convers. Congr. Expo. (ECCE)*, Oct. 2022, pp. 1–6.

[2] G. Schaible, "Understanding irrigated agriculture," USDA Statistic, Farm Practices Manag., Tech. Rep., 2017. [Online]. Available: https://www.ers.usda.gov/amber-waves/2017/june/understanding-irrigated-agriculture/

[3] D. Lightle and K. Greer, "Orchard irrigation tips," Tehama County Mobile Irrigation Lab, Tech. Rep., 2013. [Online]. Available: https://www.growingproduce.com/fruits/orchard-irrigation-tips/

[4] Ž. Despotović, M. Majstorović, M. Jovanović, and I. Stevanović, "The pressure control in irrigation 'off-grid' photovoltaic system based on mobile solar generator," *Zbornik Medunarodne Konferencije o Obnovljivim Izvorima Električne Energije-MKOIEE*, vol. 5, no. 1, pp. 245–251, 2017.

[5] J. Larabee, B. Pellegrino, and B. Flick, "Induction motor starting methods and issues," in *Proc. Rec. Conf. Papers Ind. Appl. Soc. 52nd Annu. Petroleum Chem. Ind. Conf.*, 2005, pp. 217–222.

[6] K. G. Simba, F. L. Quilumba, and N. V. Granda, "Parameter estimation of a three-phase induction motor from direct starting stator transient measurements," in *Proc. IEEE ANDESCON*, Oct. 2020, pp. 1–5.

[7] S. B. Kjaer, J. K. Pedersen, and F. Blaabjerg, "A review of single-phase grid-connected inverters for photovoltaic modules," *IEEE Trans. Ind. Appl.*, vol. 41, no. 5, pp. 1292–1306, Sep. 2005.

[8] M. N. H. Khan, M. Forouzesh, Y. P. Siwakoti, L. Li, T. Kerekes, and F. Blaabjerg, "Transformerless inverter topologies for single-phase photovoltaic systems: A comparative review," *IEEE J. Emerg. Sel. Topics Power Electron.*, vol. 8, no. 1, pp. 805–835, Mar. 2020.

[9] K. Lee, S. Lukic, and S. Ahmed, "A universal restart strategy for induction machines," in *Proc. IEEE Energy Convers. Congr. Expo. (ECCE)*, Sep. 2016, pp. 1–6.

[10] J. V. Parmar, S. K. Reddy, B. Swaminathan, A. Mudlapur, and B. Venkatesaperumal, "A novel back to back inverter configuration for solar water pumping and grid-tie application," in *Proc. IEEE Int. Conf. Environ. Electr. Eng. IEEE Ind. Commercial Power Syst. Eur. (EEEIC/I&CPS Europe)*, Jun. 2018, pp. 1–6.

[11] A. Munoz-Garcia, T. A. Lipo, and D. W. Novotny, "A new induction motor V/f control method capable of high-performance regulation at low speeds," *IEEE Trans. Ind. Appl.*, vol. 34, no. 4, pp. 813–821, 1998.

[12] S. Rahman, M. Meraj, and A. Iqbal, "Novel control algorithm for V/f control of PWAM based induction motor drive," in *Proc. 44th Annu. Conf. IEEE Ind. Electron. Soc. (IECON)*, Washington, DC, USA, Oct. 2018, pp. 3749–3754.

[13] W. Hu, Z. Wu, L. Sun, and X. Cai, "Strategy for restarting the free-running induction motor driven by a high-voltage inverter based on V/f fuzzy control," in *Proc. 8th Int. Conf. Intell. Hum.-Mach. Syst. Cybern. (IHMSC)*, Hangzhou, China, Aug. 2016, pp. 99–102.

[14] K. Lee, S. Ahmed, and S. M. Lukic, "Restart strategy for scalar (V/f) controlled synchronous reluctance machine driving a high-inertia load," *IEEE Trans. Ind. Appl.*, vol. 55, no. 4, pp. 3834–3841, Jul. 2019.

[15] K. Lee, S. Ahmed, and S. M. Lukic, "Universal restart strategy for scalar (V/f) controlled induction machines," *IEEE Trans. Ind. Appl.*, vol. 53, no. 6, pp. 5489–5495, Nov. 2017.

[16] K. Lee, H. Kim, and S. M. Lukic, "A rotating restart method for scalar (V/f) controlled synchronous reluctance machine drives using a single DC-link current sensor," *IEEE Access*, vol. 8, pp. 106629–106638, 2020.

[17] S. Shukla and B. Singh, "Single-stage PV array fed speed sensorless vector control of induction motor drive for water pumping," *IEEE Trans. Ind. Appl.*, vol. 54, no. 4, pp. 3575–3585, Jul. 2018.

[18] X. Liang and O. Ilochonwu, "Induction machine starting in practical industrial applications," *IEEE Trans. Ind. Appl.*, vol. 47, no. 1, pp. 271–280, Jan./Feb. 2011.

[19] A. Narendra, N. V. Naik, A. K. Panda, and N. Tiwary, "Modelling and analysis of grid-tied solar PV system," in *Proc. Int. Conf. Power Electron., Control Autom. (ICPECA)*, Nov. 2019, pp. 1–5.

[20] W. Li, J. Lu, H. Guo, W. Li, and X. Su, "AC contactor making speed measuring and theoretical analysis," in *Proc. 50th IEEE Holm Conf. Electr. Contacts 22nd Int. Conf. Electr. Contacts Electr. Contacts*, 2004, pp. 403–407.

[21] H. Nouri, N. Larsen, and T. S. Davies, "Contact bounce simulation using Matlab," in *Proc. 43rd IEEE Holm Conf. Electr. Contacts*, 1997, pp. 284–288.

[22] Z. Xu and L. Tang, "Digital closed loop control technology for the AC contactors," in *Proc. 27th Int. Conf. Electr. Contacts (ICEC)*, Jun. 2014, pp. 1–4.

[23] M. Kolhe, J. C. Joshi, and D. P. Kothari, "Performance analysis of a directly coupled photovoltaic water-pumping system," *IEEE Trans. Energy Convers.*, vol. 19, no. 3, pp. 613–618, Sep. 2004.

[24] S. Zhang, Z. Xu, Y. Li, and Y. Ni, "Optimization of MPPT step size in stand-alone solar pumping systems," in *Proc. IEEE Power Eng. Soc. Gen. Meeting*, Jun. 2006, pp. 1–6.

[25] M. Jayakumar and V. Rajini, "Investigation of photovoltaic water pumping system," in *Proc. Int. Conf. Circuits, Power Comput. Technol. (ICCPCT)*, Mar. 2013, pp. 275–282.

KANGBEEN LEE (Graduate Student Member, IEEE) received the B.S. degree in electrical engineering from Yonsei University, Seoul, South Korea, in 2016, and the M.S. degree in electrical engineering from Hanyang University, Seoul, in 2019. He is currently pursuing the Ph.D. degree in electrical and computer engineering with Michigan State University. He was a Research Engineer with Hyundai Motors Company, from 2016 to 2021. His research interests include high-performance electric machines and drives, multilevel/multiphase motor drives, wide bandgap device-based power electronics, and partial discharge and electromagnetic interference in AC machine drives.

MOSTAFA FEREYDOONIAN (Graduate Student Member, IEEE) received the B.Sc. degree in electrical engineering from the Abbaspour School of Engineering, Shahid Beheshti University, Tehran, Iran, in 2012. He is currently pursuing the Ph.D. degree in electrical engineering with the Department of Electrical and Computer Engineering, Michigan State University. His research interests include electric machines and high-power density drive design.

MIKAYLA BENSON (Graduate Student Member, IEEE) received the B.S. degree in mechanical and electrical engineering from Kettering University, Flint, MI, USA, in March 2020, and the M.S. degree in electrical engineering from Michigan State University, in May 2023, where she is currently pursuing the Ph.D. degree in electrical engineering. Her research interests include wide bandgap device applications, power converters, and neutral-point-less multilevel inverters.

AVINASH DORNALA (Graduate Student Member, IEEE) received the bachelor's degree in electrical and electronics engineering and the master's degree in power systems in India, in 2016. He is currently pursuing the Ph.D. degree with the Electrical Machines and Power Electronics Laboratory, Michigan State University. Since then, he has been with power generation industry in maintenance, commissioning, and erection activities in both Hydel and Thermal Power Plants.

MUSAB GUVEN (Graduate Student Member, IEEE) received the M.S. degree from North Carolina State University, in 2020. He is currently pursuing the Ph.D. degree in electrical and computer engineering with Michigan State University. His research interest includes wide bandgap devices.

YOUNSUK DONG (Member, IEEE) received the B.S., M.Sc., and Ph.D. degrees in biosystems and agricultural engineering from Michigan State University, in 2013, 2015, and 2018, respectively. He is currently an Assistant Professor with the Biosystems and Agricultural Engineering Department, Michigan State University. His research interests include improving agricultural irrigation and plant disease management using IoT-based sensor monitoring and controlling systems, computational modeling of soil-based wastewater treatment systems to understand the fate, transport, transformation of water and nutrient in soil, food processing wastewater irrigation, phosphorus recovery using iron-coated nanomaterial media, designing on-site wastewater treatment systems, and stormwater monitoring.

WOONGKUL LEE (Member, IEEE) received the B.S. degree from Yonsei University, Seoul, South Korea, in 2013, and the M.S. and Ph.D. degrees in electrical engineering from the University of Wisconsin-Madison, WI, USA, in 2016 and 2019, respectively. He was a Postdoctoral Research Associate with the Wisconsin Electric Machines and Power Electronics Consortium (WEMPEC), University of Wisconsin-Madison, from 2019 to 2020. In 2020, he joined the Department of Electrical and Computer Engineering, Michigan State University, as an Assistant Professor. His research interests include high-performance motor drive, power electronics, electric machines, and distributed energy resources.